International Journal of Mass Spectrometry 277 (2008) 91–95

Contents lists available at ScienceDirect

International Journal of Mass Spectrometry

journal homepage: www.elsevier.com/locate/ijms

Low-energy total electron scattering in the methyl halides CH_3Cl, CH_3Br and CH_3I

N.C. Jones [a], D. Field [b], J.-P. Ziesel [c,*]

[a] Institute for Storage Ring Facilities, University of Århus, Ny Munkegade, 8000 Århus C, Denmark
[b] Department of Physics and Astronomy, University of Århus, Ny Munkegade, 8000 Århus C, Denmark
[c] Laboratoire Collisions Agrégats Réactivité (CNRS-UPS UMR 5589), IRSAMC, Université Paul Sabatier, 31062 Toulouse, France

ARTICLE INFO

Article history:
Received 31 March 2008
Received in revised form 5 May 2008
Accepted 6 May 2008
Available online 15 May 2008

Keywords:
Electron–molecule interactions
Methyl halides

ABSTRACT

Absolute integral and backward total scattering cross-sections are reported for the polar molecules CH_3Cl, CH_3Br and CH_3I at electron energies from ~10 meV to 0.7 eV for backward scattering and 20 meV to 9.5 eV for integral scattering. Below 1–2 eV, the present integral cross-sections are significantly higher than data in the literature. The Born point-dipole cross-sections for rotationally inelastic scattering have been calculated and are compared with the experimental total scattering cross-sections. Discrepancies give a measure of pure elastic scattering at very low energy. Data for CH_3I demonstrate the presence of strong resonant elastic scattering and dissociative attachment at low energy.

1. Introduction

Methyl halides are the simplest of the halomethanes and have been extensively studied in low-energy electron scattering. In these polar molecules, direct rotationally inelastic scattering and vibrationally inelastic scattering through the dipolar interaction is expected to play an important role for very low-energy electron collisions, as well as direct pure elastic scattering. Resonant processes involving elastic scattering, dissociative electron attachment and vibrationally inelastic scattering may also play a significant role. Derivative electron transmission spectroscopy has been used to study attachment to temporary negative ion states [1–3]. A good deal of experimental and theoretical work has been devoted to dissociative attachment, both at room temperature [4–8]and references therein and in the heated molecule [7,9–12]. Experimental data for elastic scattering and vibrational excitation is more scarce [13–15] and very low-energy data for rotationally inelastic scattering, which we report here, are altogether lacking.

Total scattering cross-sections have been determined using electron transmission techniques for all the methyl halides presented here [3,4,16–19] but at energies above several hundred meV. We have measured total scattering in CH_3Cl, CH_3Br and CH_3I down to 20 meV and scattering into the backward hemisphere to 10 meV, with the very high electron energy resolution required to obtain accurate cross-sections in the very low-energy range.

2. Experimental

The experimental system for measuring electron scattering at the University of Århus and its modes of operation are described in detail elsewhere [20]. Briefly, synchrotron radiation from the ASTRID storage ring is used to photoionize argon at 78.66 nm, about 3 meV above the $Ar^+ {}^2P_{3/2}$ threshold. The energy resolution of the electrons is determined by the photon bandpass and is typically in the range 1–1.6 meV full-width at half-maximum. Electrons are formed into a beam and pass through a cell containing the target gas at room temperature. The intensity of the electron beam, in the presence and absence of target gas, is recorded as a function of electron energy. The total integral scattering cross-section σ_T is then calculated using

$$\sigma_T = (N\ell)^{-1} \ln\left(\frac{I_0}{I_t}\right) \quad (1)$$

where N is the gas number density, ℓ the path length of the cell and I_0 and I_t are the intensities of the incident and transmitted electron beams, respectively. In a separate experiment an axial magnetic field of 2×10^{-3} T is applied and electrons scattered in the forward hemisphere exit the collision cell and are detected while backward-scattered electrons are lost and not recorded. Thus, in the presence of the magnetic field, the measured cross-section is the backward total scattering cross-section σ_B, that is, the cross-section integrated over the 2π solid angle associated with the backward hemisphere. The energy of the electron beam is calibrated using electron scattering data for N_2 [21] and is better than ±2 meV at very low energy.

* Corresponding author. Tel.: +33 687 118431.
E-mail address: j.p.ziesel@irsamc.ups-tlse.fr (J.-P. Ziesel).

1387-3806/$ – see front matter © 2008 Elsevier B.V. All rights reserved.
doi:10.1016/j.ijms.2008.05.007

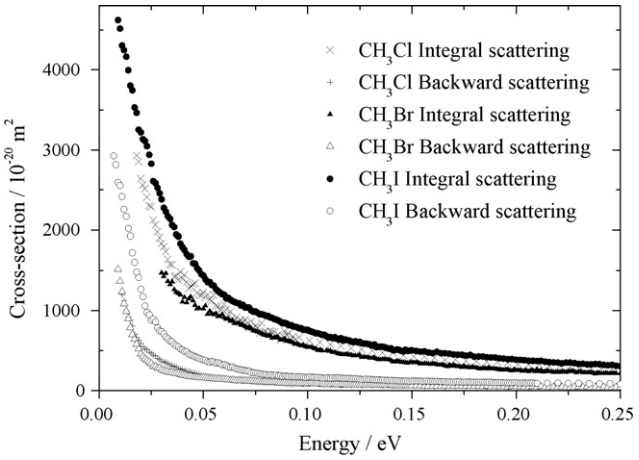

Fig. 1. A comparison of the integral scattering and backward-scattering cross-sections for CH_3Cl, CH_3Br and CH_3I.

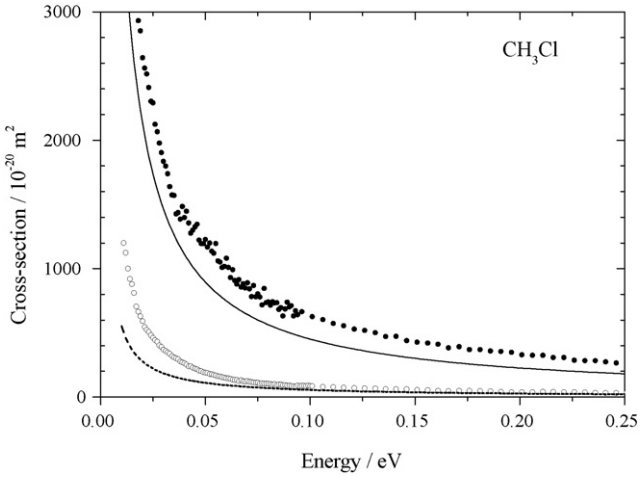

Fig. 2. Integral scattering and backward-scattering cross-sections for CH_3Cl up to 0.25 eV: (●) experiment, integral total; (○) experiment, backward total; (—) Born theory, integral rotationally inelastic; (- - -) Born theory, backward rotationally inelastic.

Uncertainties in the reported cross-sections arise from sources including pressure measurements, random fluctuations in the electron beam intensities and uncertainties in calibration of the path length of the electrons through the collision cell. These uncertainties correspond to an error of ±5% in the quoted cross-sections at all energies for scattering in the presence or absence of the magnetic field, save at the very lowest energies in the absence of the magnetic field for which a figure of ±8% is appropriate. Furthermore there are systematic errors from forward scattering in the measured total integral scattering cross-sections, as electrons scattered along the cell from up to 3° at the entrance to up to 27° at the exit are not separated from unscattered electrons [22].

3. Results and discussion

Fig. 1 shows all our data collated, so that a comparison can be made directly of the scattering behaviour of the three target species. Below we discuss data for individual species separately.

3.1. CH_3Cl and CH_3Br

In the present investigation total integral scattering cross-sections for CH_3Cl have been measured from 18 meV to 9.5 eV and backward-scattering cross-sections from 11 meV to 0.7 eV. Total integral scattering cross-sections for CH_3Br have been measured from 30 meV to 9.5 eV and backward-scattering cross-sections from 9 meV to 0.7 eV.

3.1.1. Cross-sections behaviour from very low energies up to 0.25 eV

Total integral and backward-scattering cross-sections for CH_3Cl and CH_3Br up to 0.25 eV are shown in Figs. 2 and 3. The cross-sections rise sharply from about 0.15 eV towards very low energy and also exhibit strong forward scattering. These features are characteristic of scattering in this energy range dominated by direct rotational excitation, as already observed in polar molecules such as CH_3NO_2, $C_2H_5NO_2$ and $C_6H_5NO_2$ [22]. We have performed calculations of rotationally inelastic cross-sections using the Born point-dipole approximation for electron scattering from polar symmetric top molecules [23] including all populations and transitions involved at 298 K. CH_3Cl and CH_3Br are prolate symmetric tops and the pure rotational scattering cross-section in SI units between the rotational levels (J, K) and (J', K') integrated between the two angles θ_1 and θ_2 may be expressed as

$$\sigma(J,K;J',K') = \xi(2J+1)\begin{pmatrix} J & J' & 1 \\ K & -K' & 0 \end{pmatrix}^2 \times \ln\left[\left|\frac{k^2+k'^2-2kk'\cos\theta_2}{k^2+k'^2-2kk'\cos\theta_1}\right|^{1/2}\right] \quad (2)$$

where $\xi = (4\pi/3k^2)(\mu^2/[ea_0]^2)$. In Eq. (2), J is the total angular momentum quantum number of the molecule and K its projection on the molecular axis. k and k' are the magnitudes of the initial and final wavevectors given by $k = (2m_eE)^{1/2}/\hbar$, where m_e and E are the mass and energy of the electron, $ea_0 = 8.4784 \times 10^{-30}$ Cm and μ is the dipole moment of the target molecule ($\mu(CH_3Cl) = 0.745$ au, $\mu(CH_3Br) = 0.717$ au). The Wigner 3-j symbols are evaluated using the tables given in Mizushima [24].

The energies of the rovibrational levels of the targets have been calculated, where values of J up to 100 and vibrational levels up to 1100 cm^{-1} have been included. The Boltzmann population of these levels at 298 K have then been derived. To simulate rotationally

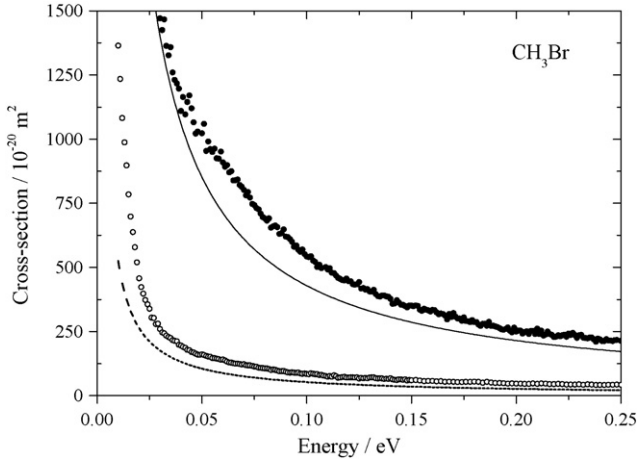

Fig. 3. Integral scattering and backward-scattering cross-sections for CH_3Br up to 0.25 eV: (●) experiment, integral total; (○) experiment, backward total; (—) Born theory, integral rotationally inelastic; (- - -) Born theory, backward rotationally inelastic.

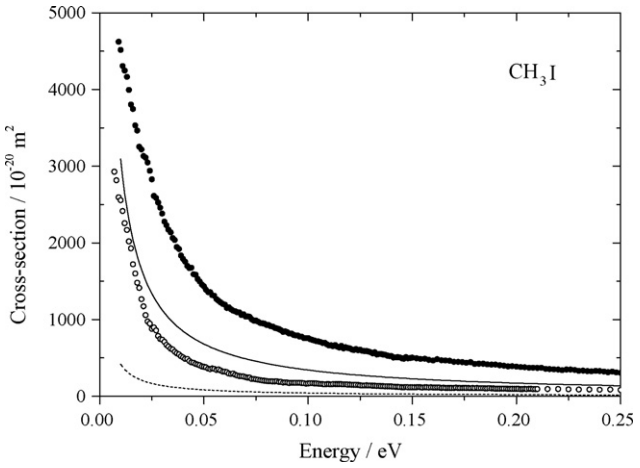

Fig. 4. Integral scattering and backward-scattering cross-sections for CH_3I up to 0.25 eV: (●) experiment, integral total; (○) experiment, backward total; (—) Born theory, integral rotationally inelastic; (- - -) Born theory, backward rotationally inelastic.

inelastic events, all contributions from the selection rules $\Delta J = 0, \pm 1$ and $\Delta K = 0$ are combined at any given energy and folded with the Gaussian energy distribution of the incident electrons. Near-axis scattering has to be omitted from the calculations of integral Born cross-sections as some of the forward scattered electrons go undetected in the experiment due to the geometry of the collision cell (see above). This problem has been treated using the method given in [25] and the procedure to obtain corrected Born cross-sections for comparison with the experimental data has been described in detail elsewhere [22,26].

The calculated effective Born cross-sections are shown with the experimental data in Figs. 2–4 as continuous (integral) and dashed lines (backward scattering). In all cases, Born theory underestimates experiment and the disagreement is most obvious in backward scattering towards the lowest energies. Such behaviour has already been noted in the halobenzenes [27]. The major reason for the discrepancy is that the Born model omits pure elastic scattering. While there are no data to estimate pure elastic scattering for the present halides, we know however from results for rotationally inelastic scattering in H_2O [28,29] that pure elastic scattering makes an increasing contribution towards the total cross-section at low energy and may approach 40% of the total below 200 meV. Our results suggest that the contribution of pure elastic scattering is comparable in the methyl halides to that in H_2O but somewhat less. The observation that the disagreement between Born values is greatest in backward-scattering stems from the fact that the collisions which give rise to backward scattering are those which probe most strongly the repulsive wall of the potential in short range interactions involving the lower partial waves. The hard wall potential makes a major contribution to elastic scattering and in H_2O in fact may lead to pure elastic dominance of the cross-sections at low energy for high angle scattering [28].

Apart from rotationally inelastic scattering and direct elastic scattering, other processes may contribute significantly to the total integral cross-sections, for example through temporary negative-ion states (TNI). In the very low-energy range, dissociative attachment, long-lived attachment, vibrational excitation, rotationally inelastic and pure elastic scattering may all occur [30] and references therein]. Dissociative attachment processes through the $CH_3X^-\ ^2A_1$ resonant state are very weak, especially in CH_3Cl where the Cl^- cross-section is estimated to be less than $10^{-26}\,m^2$ at 300 K [7,11]. For Br^-/CH_3Br, the cross-section at room temperature has been measured as $1.8 \times 10^{-22}\,m^2$ peaking at 0.38 eV [10] and extends with a slight decrease down to zero energy in the theoretical model of Wilde et al. [7]. In CH_3Br, the integral vibrational excitation cross-section ($\Delta\upsilon = +1$) for the ensemble of υ_3 modes at $T = 300$ K is estimated to peak at about $7 \times 10^{-20}\,m^2$ near the $\upsilon_3 = 1$ onset [12]. This value includes the direct excitation and the resonance contribution, as well as the interference between the direct and the resonant processes. All these processes have too low a cross-section to play a marked role at very low energy in the total scattering cross-sections in CH_3Cl and CH_3Br. This reinforces the conclusion that the major contributions to scattering are rotationally inelastic scattering and direct elastic scattering.

3.1.2. Absolute integral total electron scattering cross-sections

Absolute cross-sections for integral total scattering are reported at some selected energies from 20 meV to 9.5 eV in Table 1. Cross-sections for both CH_3Br and CH_3Cl agree within about 10% above 5 eV for data in references [3,4,16,17,19]. However at lower energies below ~1.5 eV there is pronounced disagreement with earlier work, with our cross-sections considerably higher than those previously measured. The exception to this is Shi et al. [14] who have derived total scattering cross-sections for CH_3Cl by integrating their differential elastic scattering data. They reported total cross-sections at 0.5 and 1.0 eV of $147 \times 10^{-20}\,m^2$ and $74 \times 10^{-20}\,m^2$, respectively, in very good agreement with our values of $143 \times 10^{-20}\,m^2$ and $73 \times 10^{-20}\,m^2$ at these energies. For CH_3Cl a value of $1790 \times 10^{-20}\,m^2$ has been measured for total scattering by thermal electrons at 293 K in an electron cyclotron resonance experiment [31]. This value lies about 40% lower than our value for 30 meV, taking into account the omission of forward scattering in our measurements.

Table 1
Absolute integral total scattering cross-sections in CH_3Cl and CH_3Br, in units of $10^{-20}\,m^2$

CH_3Cl			CH_3Br		
Energy (eV)	Present	[16]	Energy (eV)	Present	[17]
0.020	2643				
0.030	1836		0.030	1470	
0.050	1225		0.050	1022	
0.075	804		0.075	743	
0.1	608		0.1	543	
0.15	428		0.15	351	
0.25	269	58.2	0.25	214	
0.35	186	51.4	0.35	158	
0.45	153	46.0	0.4	136	62.6
0.55	131	41.2	0.5	111	58.0
0.65	111	38.4	0.7	85.4	53.6
0.75	92	36.5	0.9	68.5	48.9
0.85	83	35.4	1.1	58.2	47.1
1.05	73	33.5	1.3	52.0	45.4
1.25	65	32.5	1.6	46.7	45.0
1.35	64	32.2	1.8	42.5	43.8
1.45	60	31.7	2.0	41.8	43.0
1.7	55	31.6	2.5	37.8	39.4
2.0	50	31.7	3.0	36.5	39.0
2.2	49	32.0	3.5	35.8	39.0
2.5	46	32.6	4.0	34.1	38.8
3.0	45	33.4	4.5	35.4	38.6
3.5	43	34.3	5.0	34.8	40.0
4.0	43	34.7	6.0	35.5	39.7
4.5	42	34.6	7.0	35.8	40.4
5.0	41	34.5	8.0	37.4	40.4
5.5	41	34.6	9.0	35.6	39.0
6.5	39	35.3			
7.5	39	35.4			
8.5	39	35.1			
9.5	38	33.6			

3.2. CH_3I: total scattering cross-sections

In the present investigation total integral scattering cross-sections for CH_3I have been measured from 9 meV to 9.5 eV and backward-scattering cross-sections from 7 meV to 0.7 eV.

Table 2 shows a comparison of our integral total cross-section with the measurement of Krzysztofowicz and Szmytkowski [18] from 0.45 to 9.3 eV. There is very good agreement with the previous data above 6 eV, between 2 and 6 eV our values are slightly higher but the overall shape is quite similar with a broad and weak maximum centred around 5.5 eV, although 1 eV below the previous experiments [3,18]. In the very low-energy range down to 9 meV (Fig. 4), total scattering cross-sections increase sharply as in CH_3Cl and CH_3Br. However in CH_3I, forward scattering becomes increasingly less marked at very low energies, a point which we discuss below. Calculations of integral and backward rotational cross-sections in CH_3I ($\mu = 0.638$ au), in the Born point-dipole approximation, are again lower than the experimental values, as shown in Fig. 4.

Unlike in CH_3Cl and CH_3Br, the resonant CH_3I^- $^2A_1$ state may play a significant role at very low energies. This arises because CH_3I^- crosses the neutral ground state near the vibrational level $\upsilon_3 = 1$ whereas the crossing point is near $\upsilon_3 = 8$ and 4 in CH_3Cl and CH_3Br, respectively [7]. This results in a very high dissociative attachment cross-section I^-/CH_3I at room temperature, as measured at high resolution by Alajajian et al. [32] and by Schramm et al. [6]. Theoretical models for dissociative attachment in the polar molecule CH_3I have been investigated by Fabrikant and Hotop [33] and, apart from the ultra-low-energy range below 1 meV, a bound dipole-supported state of CH_3I^- appears to be involved together with the CH_3I^- resonant repulsive state. However a comparison of the I^- cross-section, measured at an electron energy resolution $\leq$1 meV [6], with our integral total cross-section (Table 2) shows that, in our energy range starting at 9 meV, the contribution of dissociative attachment to the total scattering is still minor though by no means negligible.

Our data may nevertheless be used to point very clearly to the presence of the resonant states involved in the dissociative attachment in CH_3I. As we have seen above, rotationally inelastic scattering yields strong forward scattering. Thus in CH_3Cl for example, the measured ratio, R, of backward scattering to integral scattering (less the forward cone omitted in the experiment) lies between 0.1 and 0.2 with the largest values at the lowest energies. However for CH_3I, in the presence of attachment, we do not measure the scattering cross-section into the backward hemisphere when experiments are performed in the presence of the axial magnetic field. Rather we measure a combination of events including dissociative attachment, which occurs in both the backward and forward hemispheres. Thus we find that the ratio, R, of the apparent backward-scattering cross-section to the integral rises from ~0.25 at <100 meV towards 0.5 at very low energy, with an abrupt rise below 20–25 meV. This is diagnostic of the influence of additional channels with preponderantly spherical angular scattering distributions, that is resonant elastic scattering and dissociative attachment [34].

Table 2
Absolute integral total scattering cross-sections and dissociative attachment cross-section for CH_3I, in units of 10^{-20} m^2

Energy (eV)	Present	[18]	I^-/CH_3I [6]	Energy (eV)	Present	[18]
0.010	4516		141.7	1.35	67	55.3
0.020	3219		89.6	1.45	70	53.1
0.030	2384		77.0	1.65	62	51.3
0.040	1790		82.2	1.85	57	50.2
0.050	1434		105.1	2.0	61	49.7
0.060	1196		134.9	2.2	61	49.7
0.065	1107		29.8	2.4	59	49.8
0.070	1039		21.2	2.6	58	50.0
0.080	933		19.4	2.8	59	49.7
0.100	759		17.0	3.0	58	49.5
0.125	607		13.9	3.3	58	50.4
0.130	575		7.5	3.8	58	51.1
0.135	550		6.2	4.3	58	52.6
0.160	466		6.4	4.8	60	54.1
0.25	305			5.3	60	55.6
0.45	184	95.8		5.6	59	56.2
0.55	151	85.8		5.8	60	56.9
0.65	126	80.3		6.1	58	57.8
0.70	125	76.4		6.3	59	58.0
0.80	109	72.1		6.8	59	58.1
0.90	99	68.5		7.3	58	57.6
1.0	88	64.2		7.8	57	56.2
1.1	81	61.7		8.3	56	55.2
1.2	79	57.9		8.8	55	54.8
1.25	74	56.0		9.3	56	54.2

4. Concluding remarks

Our results report scattering data in an energy regime below 100 meV which has not been explored in previous work on this basic group of simple organic species. The very high cross-sections found for rotationally inelastic scattering emphasise the importance of polar molecules in determining the electron energy distribution within cool plasmas. An important advance, that is presently being made, is to apply the theory described in [29] to obtain accurate state-to-state rotationally inelastic cross-sections from experimental data for CH_3Cl and CH_3Br and elastic scattering cross-sections. This will give an accurate assessment of the relative amount of pure elastic and rotationally inelastic scattering at any energy.

Acknowledgements

We thank the Director and staff of the Institute for Storage Ring Facilities at the University of Århus for their provision of synchrotron radiation facilities on the ASTRID storage ring. JPZ thanks the CNRS (France) and the FNU (Denmark) for support under the European Science Exchange Programme and the EU under the Transnational Access to Major Research Infrastructures Programme (Contract no. HPRI-CT-2001-00122). The authors are grateful to H. Hotop, M.-W. Ruf, I.I. Fabrikant and M. Allan for providing their CH_3I data in numerical form.

References

[1] P.D. Burrow, A. Modelli, N.S. Chiu, K.D. Jordan, J. Chem. Phys. 77 (1982) 2699.
[2] A. Modelli, F. Scagnaroli, G. Distefano, D. Jones, M. Guerra, J. Chem. Phys. 96 (1992) 2061.
[3] A. Benitez, J.H. Moore, J.A. Tossell, J. Chem. Phys. 88 (1988) 6691.
[4] H.-X. Wan, J.H. Moore, J.A. Tossell, J. Chem. Phys. 94 (1991) 1868.
[5] D.M. Pearl, P.D. Burrow, J. Chem. Phys. 101 (1994) 2940.
[6] A. Schramm, I.I. Fabrikant, J.M. Weber, E. Lebert, M.-W. Ruf, H. Hotop, J. Phys. B: At. Mol. Opt. Phys. 32 (1999) 2153.
[7] R.S. Wilde, G.A. Gallup, I.I. Fabrikant, J. Phys. B: At. Mol. Opt. Phys. 33 (2000) 5479.
[8] G.A. Gallup, I.I. Fabrikant, Phys. Rev. A 75 (2007) 032719.
[9] D. Spence, G.J. Schulz, J. Chem. Phys. 58 (1973) 1800.
[10] P.G. Datskos, L.G. Christophorou, J.G. Carter, J. Chem. Phys. 97 (1992) 9031.
[11] D.M. Pearl, P.D. Burrow, I.I. Fabrikant, G.A. Gallup, J. Chem. Phys. 102 (1995) 2737.
[12] M. Braun, I.I. Fabrikant, M.-W. Ruf, H. Hotop, J. Phys. B: At. Mol. Opt. Phys. 40 (2007) 659.
[13] X. Shi, T.M. Stephen, P.D. Burrow, J. Chem. Phys. 96 (1992) 4037.
[14] X. Shi, V.K. Chan, G.A. Gallup, P.D. Burrow, J. Chem. Phys. 104 (1996) 1855.
[15] M. Allan, I.I. Fabrikant, J. Phys. B: At. Mol. Opt. Phys. 35 (2002) 1025.
[16] A.M. Krzysztofowicz, C. Szmytkowski, J. Phys. B: At. Mol. Opt. Phys. 28 (1995) 1593.
[17] A.M. Krzysztofowicz, C. Szmytkowski, Chem. Phys. Lett. 219 (1994) 86.

[18] C. Szmytkowski, A.M. Krzysztofowicz, Chem. Phys. Lett. 209 (1993) 474.
[19] M. Kimura, O. Sueoka, C. Makochekanwa, H. Kawate, M. Kawada, J. Chem. Phys. 115 (2001) 7442.
[20] S.V. Hoffmann, S.L. Lunt, N.C. Jones, D. Field, J.-P. Ziesel, Rev. Sci. Instrum. 73 (2002) 4157.
[21] R.E. Kennerly, Phys. Rev. A 21 (1980) 1876.
[22] S.L. Lunt, D. Field, J.-P. Ziesel, N.C. Jones, R.J. Gulley, Int. J. Mass Spectrom. 205 (2001) 197.
[23] O.H. Crawford, J. Chem. Phys. 47 (1967) 1100.
[24] M. Mizushima, Quantum Mechanics of Atomic Spectra and Atomic Structure, Benjamin, New York, 1970.
[25] K. Floeder, D. Fromme, W. Raith, A. Schwab, G. Sinapius, J. Phys. B: At. Mol. Opt. Phys. 18 (1985) 3347.
[26] R.J. Gulley, T.A. Field, W.A. Steer, N.J. Mason, S.L. Lunt, J.-P. Ziesel, D. Field, J. Phys. B: At. Mol. Opt. Phys. 31 (1998) 5197.
[27] S.L. Lunt, D. Field, S.V. Hoffmann, R.J. Gulley, J.-P. Ziesel, J. Phys. B: At. Mol. Opt. Phys. 32 (1999) 2707.
[28] A. Faure, J.D. Gorfinkiel, J. Tennyson, J. Phys. B: At. Mol. Opt. Phys. 37 (2004) 801.
[29] R. Čurik, J.-P. Ziesel, N.C. Jones, T.A. Field, D. Field, Phys. Rev. Lett. 97 (2006) 123202.
[30] H. Hotop, M.-W. Ruf, M. Allan, I.I. Fabrikant, in: B. Bederson, H. Walther (Eds.), Advances in Atomic and Molecular and Optical Physics, vol. 49, Academic Press, New York, 2003, p. 85.
[31] A.A. Christodoulides, R. Schumacher, R.N. Schindler, J. Phys. Chem. 79 (1975) 1904.
[32] S.H. Alajajian, M.T. Bernius, A. Chutjian, J. Phys. B: At. Mol. Opt. Phys. 21 (1988) 4021.
[33] I.I. Fabrikant, H. Hotop, Phys. Rev. A 63 (2001) 022706.
[34] D. Field, N.C. Jones, J.-P. Ziesel, Phys. Rev. A 69 (2004) 052716.